Absolute determination of optical constants of three transition metals using reflection electron energy loss spectroscopy

H. Xu,[1,2] L. H. Yang,[1,2] J. Tóth,[3] K. Tőkési,[3,4] B. Da,[5] and Z. J. Ding[1,2,a)]
[1]*Key Laboratory of Strongly-Coupled Quantum Matter Physics, Chinese Academy of Sciences, Hefei 230026, China*
[2]*Department of Physics, University of Science and Technology of China, Hefei 230026, China*
[3]*Institute for Nuclear Research, Hungarian Academy of Sciences (ATOMKI), Debrecen, Hungary*
[4]*ELI-ALPS, ELI-HU Non-Profit, Ltd., Dugonics tér 13, H-6720 Szeged, Hungary*
[5]*Center for Materials Research by Information Integration (CMI2), Research and Services Division of Materials Data and Integrated System (MaDIS), National Institute for Materials Science (NIMS), 1-2-1 Sengen, Tsukuba, Ibaraki 305-0047, Japan*

(Received 4 November 2017; accepted 13 January 2018; published online 26 January 2018)

The optical constants, n and k, of three transition metals (Cr, Co, and Pd) were determined from the measured reflection electron energy-loss spectroscopy (REELS) spectra, covering the spectral energy range from visible to vacuum ultraviolet. To do this, a spectral data analysis technique [Xu *et al.*, Phys. Rev. B **95**, 195417 (2017)], which combines a sophisticated Monte Carlo simulation for modelling the experimental REELS spectrum and the simulated annealing algorithm for the determination of the true energy loss function (ELF) was adopted. The validity of the obtained ELFs was discussed by comparing with the previous data derived by optical methods and by applying the oscillator strength and the perfect screening-sum rules. Besides, the consistency of the calculated data was evaluated for three *in situ* measurements for each sample at three primary energies. The complex dielectric function, the refractive index n and the extinction coefficient k were then derived from the obtained ELF via the analytical Kramers-Kronig relation. *Published by AIP Publishing.* https://doi.org/10.1063/1.5012013

I. INTRODUCTION

The optical constants and the dielectric function are defined by the response of the electrons of a solid to an external electric field. Such information has fundamental importance in both theoretical studies and practical applications of materials. To measure the optical properties of solids, typical sources of external fields are supplied either by light beam or by monochromatic electrons.[1,2] Three of the most widely used optical methods with a light beam are reflection spectroscopy, absorption spectroscopy and spectroscopic ellipsometry. These methods are based on Fresnel relations for the reflection and transmission of radiation at a flat and smooth interface between two media. The corresponding commercial equipment is available in many laboratories. However, the measurements are sensitive to surface roughness and surface contamination, while they are usually performed under atmospheric conditions, where surface cleanliness is not guaranteed. Therefore, the accuracy of the optical constants obtained by reflection or ellipsometry measurements is limited. For example, the accuracy of the optical properties of Cr can be strongly influenced in an optical measurement, because of its easy oxidizing property. In addition, the energy region and the range of the measured optical constants are directly constrained by the light source, where photon energies are usually below 6.5 eV. Further investigations at higher photon energies, like for example, in the vacuum ultraviolet (VUV) region, would require complex facilities, such as, a synchrotron radiation source and an ultra-high vacuum (UHV), which makes the laboratory measurement difficult. These drawbacks can be overcome by applying electron probe techniques, such as, electron energy-loss spectroscopy (EELS). EELS is routinely carried out under UHV conditions and is not as sensitive to the surface roughness as the optical reflection or ellipsometry experiment. Being the intrinsic property of a sample, the optical constants are independent of the primary energy of an EELS spectrum. Therefore, the optical constants of a solid can be determined from a single EELS spectrum measured at one incident energy, where the energy loss corresponds to the photon energy of the obtained optical constants.

Historically, firstly, the EELS at the transmission mode was studied[3–5] for extracting the optical data. Since transmission EELS requires very high incident beam energy (tens or hundreds of keV) and a very thin (less than 200 nm) and free-standing film sample, reflection EELS (REELS) has attracted more interest for its simplicity of measurement. In REELS, the typical primary energy of the electron beam is about thousands of eV. Usually, the surface chemical analysis techniques, such as, x-ray photoelectron spectroscopy and Auger electron spectroscopy, can also be easily integrated into the experimental setup. In addition, there is no special requirement for sample preparation. Despite the merits of REELS, one main issue of the technique is about the quantitative interpretation of the measured spectrum which is more complex than the case of the transmission EELS. At energies about keV, and under the oblique incidence and detection

a)Author to whom correspondence should be addressed: zjding@ustc.edu.cn

geometry of experimental configuration, the surface excitation effect of electron inelastic scattering and multiple scattering effects should be significant, which complicate to a great extent the theoretical modeling of a REELS spectrum related to optical data. To derive the photon energy ($\Delta E = \hbar\omega$) or frequency, and ω-dependent optical constants from a measured REELS spectrum, it is necessary to establish an accurate theoretical model of the dielectric function $\varepsilon(\omega)$, or specifically, the bulk energy loss function (ELF), $\mathrm{Im}[-1/\varepsilon(\omega)]$, from the REELS spectrum.

To our knowledge, the first attempt to extract optical constants from REELS spectra was performed by Ohno,[6] where as a coarse approximation, i.e., the ELF being proportional to the REELS spectral intensity was assumed. Later, many works[7–15] have been done on this issue. As was mentioned before, an accurate description of a REELS spectrum requires careful consideration on two aspects, namely the surface excitation effect of electron inelastic scattering and multiple scattering effects for both electron inelastic and elastic scattering processes. By assuming homogeneous scattering properties of a solid, a formula was derived by Tougaard and Chorkendorff,[16] which allows determination of the energy loss distribution of a single inelastic scattering from an EELS spectrum. This algorithm was adopted by several authors[7–9,15] for removing the multiple scattering effect, although the homogeneous sample assumption is not fulfilled for the REELS experiment because of the existence of surface excitations. The REELS spectrum was analytically expressed as a multi-convolution of a single inelastic scattering distribution for bulk excitation, i.e., the differential inverse inelastic mean free path (DIIMFP), by excluding the elastic scattering. To account for the elastic scattering effect, a modification was then made[10,11] by simply applying a scaling factor to the Landau formulation, which is called recently as the extended Landau method. In this way, an effective ELF with ambiguous physical meaning, which in fact embodies both the features of bulk and surface excitations, can be obtained. To further deal with the surface excitation problem, Werner has introduced two components,[12,17,18] i.e., a bulk and a surface energy loss distribution function, into a single inelastic scattering distribution. Apart from the homogenous sample assumption,[16] Werner's algorithm also requires pre-knowledge of the electron inelastic mean free path (IMFP) and the surface excitation parameter (SEP) as input parameters, which implies logical contradiction if the algorithm is not performed self-consistently, since such parameters should be determined by the ELF of the sample. A more reasonable formula relating the ELF and the DIIMFP of a sample was derived by Yubero and Tougaard (YT-model).[19,20] Using this technique, the optical constants of Fe, Pd and Ti were recently studied.[15] The accuracy of the YT-model is, however, questionable due to two main assumptions of the model. The first assumption lies in the procedure to determine the effective single scattering cross-section by employing Tougaard and Chorkendorff's algorithm,[16] where the extracted cross-section is not strictly the single scattering cross-section taken into account for a homogenous sample. Secondly, the electron trajectory was assumed to be of V-shape,[21] where only a single elastic scattering event happens along the trajectory. Most importantly, all these works that attempted to describe a REELS spectrum with analytical formulas cannot provide absolute values of optical constants. A scaling procedure is always required to determine the absolute value by resorting to either the perfect-screening (*ps*)- sum rule or/and the oscillator-strength (*f*)- sum rule, which are used in a similar sense as a normalization procedure. Although the optical constants obtained by the YT-model behave satisfactorily in reproducing the cross-sections derived from the measured REELS spectra at several primary energies,[22–24] we will show that the evaluation of the *f*-sum rule has poor agreement with the theoretical expectation.

As a special data analysis method of the measured REELS spectrum, Da *et al*. have developed a reverse Monte Carlo (RMC) technique[14] to obtain the energy loss function and the optical constants of the target materials. The Monte Carlo (MC) method was employed to accurately account for the elastic and multiple scattering effects, and the surface excitation effect was also partially included with an extra term. Mott's cross-section[25,26] and a dielectric functional approach were used for the description of electron elastic scattering and inelastic scattering, respectively. As an example, and showing the virtue of the model, the optical constants of SiO_2 in absolute values were then obtained in their work with acceptable errors, i.e., -14.72% and 0.9%, respectively, for the *f*- and *ps*-sum rules. The relatively poor *f*-sum rule value was mostly attributed to a rough treatment for the surface excitation, which was partially accounted for by simply adding a surface ELF term, $\mathrm{Im}[-1/(\varepsilon+1)]$, to the bulk excitation distribution, which is proportional to the bulk ELF, $\mathrm{Im}[-1/\varepsilon]$. This approximation had been demonstrated to be poor by Yubero and Tougaard,[27] but the work of Da *et al*.[14] has indicated that the RMC method by a self-consistent computation of optical constants from an experimental spectrum can, in principle, work quite reasonably to present an absolute value without the help of the sum rule normalization procedure.

Recently, the RMC method was further improved by a more exact physical modeling of the surface effect,[28,29] where the inhomogeneous surface excitation for electron inelastic scattering in a vacuum and a sample near the surface was considered with a depth dependent DIIMFP by a semi-classical approach.[30,31] The method has been then successfully applied to determine the absolute values of the ELFs of two transition metals (Fe[28] and Ni[29]), where the sum rule check was evaluated with very good agreement with the theoretical values. In analogy to the mature technique of optical methods, the newly developed RMC method can directly and rather accurately provide absolute values of the desired optical constants from the measured REELS spectra, where no artificial scaling factor is employed.

In this work, the energy loss function and the optical constants of chromium, cobalt and palladium were determined with the help of the newly developed RMC method in the photon energy range of 0–120 eV. Comparisons were made between the present results and those by other models. To verify the reliability and the consistency of the present method, *in situ* measurements of REELS spectra for each sample at three primary energies were performed. The accuracy of the ELF and optical constant calculations was

verified by evaluating the oscillator-strength *f*-sum rule in two forms and the perfect screening, *ps*-sum rule.

II. EXPERIMENT

The three transition metals (Cr, Co, Pd) were prepared as polycrystalline sheets, which were mechanically polished before being moved to the measurement chamber. REELS spectra of the Cr and Co samples were recorded at primary electron energies of 1000, 2000 and 3000 eV, and those of the Pd sample were recorded at primary electron energies of 2000, 3000 and 4000 eV in an energy loss range of 0–120 eV, by a home-built electron spectrometer (ESA-31) in ATOMKI.[32] The sample surface was cleaned with Ar^+ ion etching at 3 keV with the beam intensity of 40 μA/cm^2 for 1–2 min before each measurement. The incident angle of the Ar^+ ion beam was 40° relative to the surface normal. The analyzer works in a fixed retardation ratio mode with a relative energy resolution of 5×10^{-3}. In the present experiment, pass energies of the hemispherical electron analyzer were around 100 eV, and in this way, the analyzer energy resolution was about 0.5 eV. The full widths at half maximum, being the convolution of the analyzer and the electron source generated widening of the elastic peak, were around 0.6–0.7 eV. The REELS spectra were recorded with electron incident and exit angles of 50° and 0° with respect to the surface normal of the sample. The energy calibration was done with high accuracy with the help of XPS using atomic standards of Cu, Ag, and Au with the binding energy values of photoelectron lines of Cu $2p_{3/2}$ at 932.67 eV, Ag $3d_{5/2}$ at 368.26 eV, and Au $4f_{7/2}$ at 83.98 eV.[33,34] The measurement time at each primary energy was about 30–35 min, during which the surface cleanness was checked by XPS in several cases after the REELS measurements. From the XPS, C 1s, O 1s and Ar 2p peaks demonstrate surface contamination of no more than 2.5 at. % (relative to the sample). The vacuum level during the measurements was maintained stable at about 1.5×10^{-9} mbar.

III. THEORETICAL METHODS

A. MC modeling of electron elastic and inelastic scattering

The main features of the physical model for the MC simulation of an electron transport process in a REELS experiment are the use of Mott's cross-section for describing electron elastic scattering and a dielectric functional approach for electron inelastic scattering.

The relativistic expression of electron-atom scattering, i.e., Mott's cross-section, is given by[25,26]

$$\frac{d\sigma}{d\Omega} = |f(\vartheta)|^2 + |g(\vartheta)|^2, \tag{1}$$

where the scattering amplitudes

$$f(\vartheta) = \frac{1}{2iK}\sum_{\ell=0}^{\infty}\left\{(\ell+1)\left(e^{2i\delta_\ell^+}-1\right)+\ell\left(e^{2i\delta_\ell^-}-1\right)\right\}P_\ell(\cos\vartheta)$$
$$g(\vartheta) = \frac{1}{2iK}\sum_{\ell=1}^{\infty}\left\{-e^{2i\delta_\ell^+}+e^{2i\delta_\ell^-}\right\}P_\ell^1(\cos\vartheta) \tag{2}$$

are calculated by a partial wave expansion method,[35] where $P_\ell(\cos\vartheta)$ and $P_\ell^1(\cos\vartheta)$ are the Legendre and the first-order associate Legendre functions, and δ_ℓ^+ and δ_ℓ^- are the spin-up and spin-down phase shifts of ℓ th partial wave, respectively. Here, Thomas-Fermi Dirac atomic potential is employed in the calculation,[36] and the atomic number of the sample is the only input.

For an electron inelastic scattering process, several theories have been derived to deal with the surface excitations.[19,20,31,37–43] In order to judge the validity of the available theoretical methods, an evaluation of two typical models based on a semi-classical approach[36] and a quantum mechanical approach[38] was carried out.[30] From this calculation, one can conclude that the semi-classical approach can provide as good agreement as the quantum mechanical approach in most of the experimental conditions for the simulation of the REELS spectrum. Thus, we adopted the semi-classical model in our calculation because it has much higher computation efficiency than the quantum mechanical one.

In the adopted semi-classical model for surface excitation, the depth dependent differential inelastic cross-section, i.e., DIIMFP, where the bulk ELF and the surface ELF are incorporated in a rather complex way, is given by

$$\begin{aligned}\sigma(z) = {} & \frac{2}{\pi v^2}\int_{q_-}^{q_+} dq \frac{1}{q}\mathrm{Im}\left[\frac{-1}{\varepsilon(\mathbf{q},\omega)}\right]\Theta(-z) \\ & + \frac{4\cos\alpha}{\pi^3}\int_{q_-}^{q_+} dq \int_0^{\frac{\pi}{2}} d\theta \int_0^{2\pi} d\phi \frac{q\sin^2\theta\cos(q_\perp z)\exp(q_\parallel z)}{\tilde{\omega}^2+q_\parallel^2 v_\perp^2} \\ & \times\left\{\mathrm{Im}\left[\frac{-1}{\varepsilon(\mathbf{q}_\parallel,\omega)+1}\right]-\frac{1}{2}\mathrm{Im}\left[\frac{-1}{\varepsilon(\mathbf{q}_\parallel,\omega)}\right]\right\}\Theta(-z) \\ & + \frac{4\cos\alpha}{\pi^3}\int_{q_-}^{q_+} dq \int_0^{\frac{\pi}{2}} d\theta \int_0^{2\pi} d\phi \frac{q\sin^2\theta\exp(-q_\parallel z)}{\tilde{\omega}^2+q_\parallel^2 v_\perp^2} \\ & \times\mathrm{Im}\left[\frac{-1}{\varepsilon(\mathbf{q}_\parallel,\omega)+1}\right]\left[2\cos\left(\frac{\tilde{\omega}z}{v\cos\alpha}\right)-\exp(-q_\parallel z)\right]\Theta(z) \\ & v_\perp > 0 \end{aligned} \tag{3}$$

and

$$\begin{aligned}\sigma(z) = {} & \frac{2}{\pi v^2}\int_{q_-}^{q_+} dq \frac{1}{q}\mathrm{Im}\left[\frac{-1}{\varepsilon(\mathbf{q},\omega)}\right]\Theta(-z) \\ & + \frac{4\cos\alpha}{\pi^3}\int_{q_-}^{q_+} dq \int_0^{\frac{\pi}{2}} d\theta \int_0^{2\pi} d\phi \frac{q\sin^2\theta\cos(-q_\perp z)\exp(-q_\parallel z)}{\tilde{\omega}^2+q_\parallel^2 v_\perp^2} \\ & \times\mathrm{Im}\left[\frac{-1}{\varepsilon(\mathbf{q}_\parallel,\omega)+1}\right]\Theta(z) + \frac{4\cos\alpha}{\pi^3}\int_{q_-}^{q_+} dq \\ & \times\int_0^{\frac{\pi}{2}} d\theta \int_0^{2\pi} d\phi \times \frac{q\sin^2\theta\exp(q_\parallel z)}{\tilde{\omega}^2+q_\parallel^2 v_\perp^2} \\ & \times\left\{\mathrm{Im}\left[\frac{-1}{\varepsilon(\mathbf{q}_\parallel,\omega)+1}\right]-\frac{1}{2}\mathrm{Im}\left[\frac{-1}{\varepsilon(\mathbf{q}_\parallel,\omega)}\right]\right\} \\ & \times\left[2\cos\left(\frac{\tilde{\omega}z}{v\cos\alpha}\right)-\exp(-q_\parallel z)\right]\Theta(-z) \quad v_\perp < 0 \end{aligned} \tag{4}$$

for an electron penetrating the surface from the solid/vacuum side into the vacuum/solid side, respectively, where $\tilde{\omega} = \omega - qv\sin\theta\cos\phi\sin\alpha$, $q_{\parallel} = q\sin\theta$, and $v_{\perp} = v\cos\alpha$, α is the angle between the interface normal and the electron moving direction. The upper and lower limits of the integrals are $q_{\pm} = \sqrt{2E} \pm \sqrt{2(E-\omega)}$. Details of the derivations were elaborated in Ref. 30.

One may note that Eqs. (3) and (4) also take into account the so called Begrezungs effect which is due to the presence of the boundary, i.e., the surface.[44,45] It reduces the bulk losses compared to the case of an electron travelling through an unbounded medium. The physical meaning of the Begrezungs effect is that the excitation of surface modes takes place at the expense of the excitation of bulk modes. The total energy loss probability for the bulk excitation is thus smaller than that of an infinite medium. To get a bulk plasmon excitation probability which is positive, the negative bulk correction, $-\frac{1}{2}\mathrm{Im}[-1/\varepsilon(\mathbf{q}_{\parallel},\omega)]$ in Eqs. (3) and (4), from the boundary effect has to be balanced by the infinite bulk term.

B. Data analysis procedure of RMC

To obtain the true ELF of a solid from an experimental REELS spectrum, a trial ELF is parameterized as a sum of N Drude-Lindhard terms as

$$\mathrm{Im}\left[\frac{-1}{\varepsilon(q,\omega)}\right] = \sum_{i=1}^{N} A_i \mathrm{Im}\left[\frac{-1}{\varepsilon(q,\omega;\omega_{pi},\gamma_i)}\right], \tag{5}$$

where the $3N$ oscillator parameters, A_i, ω_{pi}, and γ_i are the oscillator strength, the energy, and the width of the i-th oscillator, respectively. They are initially arbitrarily selected at the long wavelength limit, $q \to 0$. For finite q-values, the dielectric function $\varepsilon(q,\omega)$ is extended from the long wavelength limit, namely the optical dielectric function $\varepsilon(\omega)$, via Ritchie and Howie's scheme.[46] Utilizing the initial ELF, the REELS spectrum can be simulated by employing the MC simulation method for electron transport. A goodness function of the ELF can be defined as the summed difference between the simulated spectrum and the experimental spectrum. Consequently, the problem to find the true ELF of a sample becomes the question to find the optimum set of $3N$ oscillator parameters, where N is taken to be about 50–70, which yields a minimum value of the goodness function and corresponds to the desired real ELF. To solve such a global optimization problem in $3N$ hyperspace, an evolution strategy[28] for the trial ELF was carried out by adopting a simulated annealing (SA) method[47] which is a powerful algorithm for the global optimization. As a basic property of the Metropolis importance sampling employed in the SA method, the final equilibrium state of evolution is independent of the initial state. Therefore, as mentioned, oscillator parameters of the initial ELF can, in principle, be arbitrarily assigned; but practically, in order to accelerate the warming up of the computation leading to equilibrium, they are initially estimated from the available optical constants if any.

Once the final ELF, $\mathrm{Im}[-1/\varepsilon(\omega)]$, is obtained by the RMC method, the corresponding real part, $\mathrm{Re}[-1/\varepsilon(\omega)]$, can be deduced via Kramers-Kronig relation. Then, the complex dielectric function can be expressed as

$$\begin{aligned}\varepsilon_1 &= \frac{-\mathrm{Re}\left[-1/\varepsilon(\omega)\right]}{\mathrm{Im}\left[-1/\varepsilon(\omega)\right]^2 + \mathrm{Re}\left[-1/\varepsilon(\omega)\right]^2},\\ \varepsilon_2 &= \frac{\mathrm{Im}\left[-1/\varepsilon(\omega)\right]}{\mathrm{Im}\left[-1/\varepsilon(\omega)\right]^2 + \mathrm{Re}\left[-1/\varepsilon(\omega)\right]^2}.\end{aligned} \tag{6}$$

The refractive index $n(\omega)$ and the extinction coefficient $k(\omega)$ can be thus obtained by

$$\begin{aligned}n &= \sqrt{\frac{\varepsilon_1 + \sqrt{\varepsilon_1^2 + \varepsilon_2^2}}{2}},\\ k &= \sqrt{\frac{-\varepsilon_1 + \sqrt{\varepsilon_1^2 + \varepsilon_2^2}}{2}}.\end{aligned} \tag{7}$$

IV. RESULTS AND DISCUSSION

For comparison with the experimental spectrum, the simulated raw REELS spectrum was convoluted with a Gaussian function corresponding to the experimental energy resolution, where the parameters of the Gaussian functions are chosen to mimic the elastic peak shape of the experimental spectrum. Once the simulated REELS spectrum based on the trial ELF agrees with the experimental spectrum, then the convergence condition with the "goodness" function in Ref. 28 is fulfilled and the final ELF is thus determined in the oscillator parameter space. An intuitionistic view of the evolution process can be seen in our previous work;[28] here, we just present the final results.

Since the complex dielectric function $\varepsilon(\omega)$ is principally not related to the experimental conditions, the ELF should not be dependent on the primary energy of the incident electron beam. To verify that this demand is satisfied in our data analysis, REELS measurements were performed at three primary energies, at 1000, 2000 and 3000 eV for Cr and Co and at 2000, 3000 and 4000 eV for Pd, in a wide energy loss range from the infrared to the ultraviolet. The final simulated REELS spectra are compared and presented in Figs. 1(a)–3(a) for each element. For comparison, the simulated and measured spectra were all normalized to the height of the elastic peak (i.e., zero-loss peak). It is worth mentioning that the theoretical spectra have been convoluted Gaussian functions, which fit exactly with the experimental elastic peak, as shown by the inset of Figs. 1(a)–3(a). The ELF obtained from the spectrum at each primary energy was displayed in Figs. 1(b)–3(b), in the same energy loss range. The agreement among the ELFs at the three energies is very good for all three elements.

A. Chromium

As is shown in Fig. 1(b), ELFs obtained from the experimental REELS spectra excited at the primary energies of 1000, 2000 and 3000 eV are almost the same in the whole energy loss region studied. In the case of 3000 eV, the ELF has negligible minor deviations compared to the results of

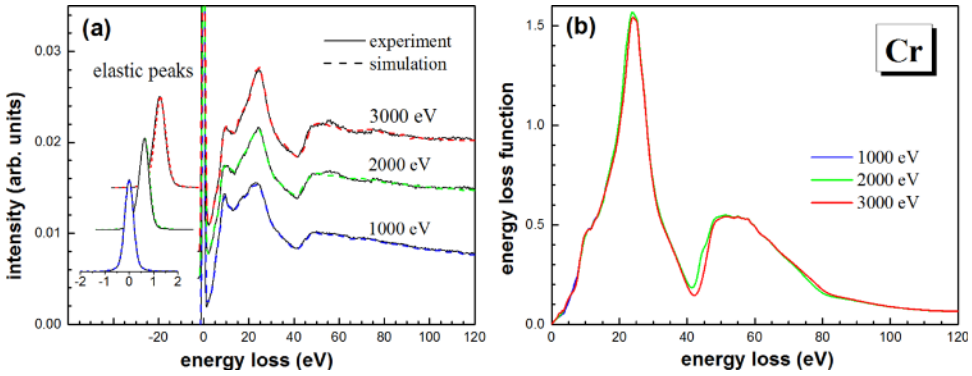

FIG. 1. (a) The final simulated REELS spectra (solid lines) of chromium at 1000, 2000 and 3000 eV, in comparison with experimental results (dash lines). (b) The final energy loss functions, $\mathrm{Im}[-1/\varepsilon(\omega)]$, obtained from the REELS spectra.

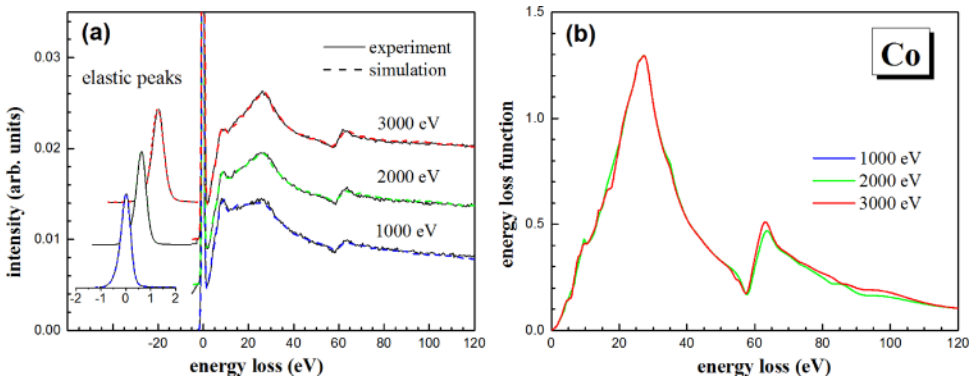

FIG. 2. (a) The final simulated REELS spectra (solid lines) of cobalt at 1000, 2000 and 3000 eV, in comparison with experimental results (dash lines). (b) The final energy loss functions, $\mathrm{Im}[-1/\varepsilon(\omega)]$, obtained from the REELS spectra.

1000 and 2000 eV, in the $M_{2,3}$-edge peak (43 eV) and in the highest plasmon peak near 24 eV. Such good agreement is expected for a successful model. The slight differences may arise from random fluctuations of the experimental spectrum, the surface roughness and the possible small contamination of the sample. Reducing the uncertainty, the three ELFs in Fig. 1(b) were averaged to form a mean ELF. To examine the obtained ELF, a comparison with available experimental data is shown in Fig. 4. Like the case of many other metals, Palik's database of optical data always lack some data in the vacuum ultraviolet region. Our ELF data generally agree well with Palik's data as well as Henke's data in the high energy loss region above the M_1-edge (74 eV). Deviations mainly occur at the peak around 9 eV and at the $M_{2,3}$-edge peak (43 eV). Since chromium oxidizes readily and the optical measurements were not performed under high vacuum conditions, such discrepancy can be attributed to the presence of chromium oxides during the measurement.

To do further investigation of the obtained ELFs and the related optical constants, the oscillator-strength (f) sum rule in two forms

$$Z_{eff}|_{\mathrm{ELF}} = \frac{2}{\pi\Omega_p^2}\int_0^\infty \omega \mathrm{Im}\left[-1/\varepsilon(\omega)\right] d\omega, \tag{8}$$

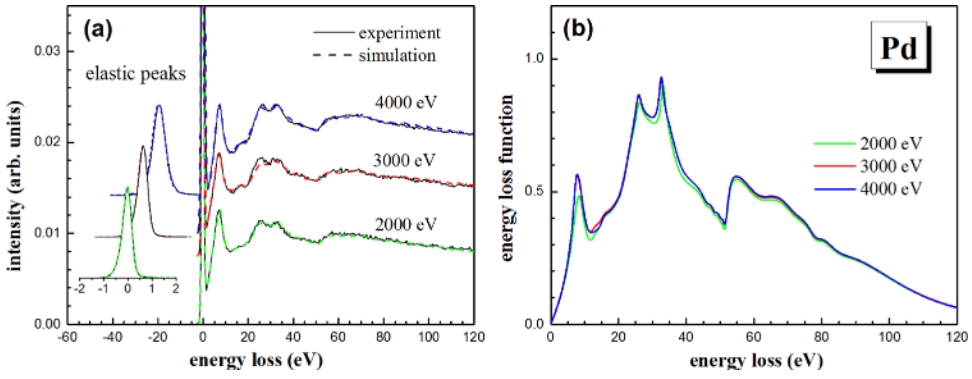

FIG. 3. (a) The final simulated REELS spectra (solid lines) of palladium at 2000, 3000 and 4000 eV, in comparison with experimental results (dash lines). (b) The final energy loss functions, $\mathrm{Im}[-1/\varepsilon(\omega)]$, obtained from the REELS spectra.

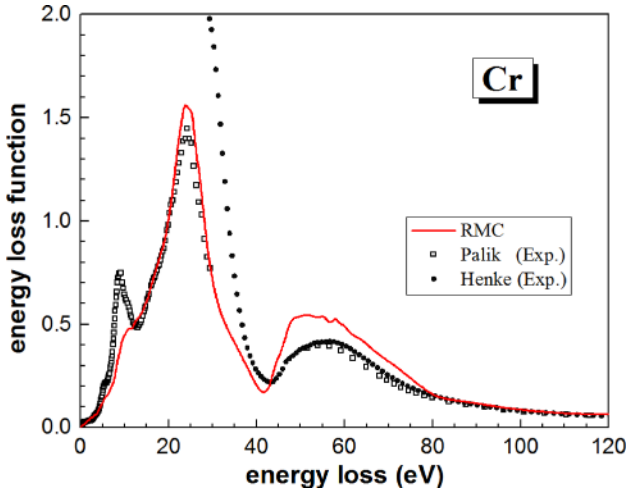

FIG. 4. Comparison for the ELFs of Cr. Red line: present results obtained from REELS measurement by the RMC method; open square: from the optical measurements compiled in Palik's database;[2] solid circles: from Henke's atomic scattering factors.[48]

$$Z_{eff}|_k = \frac{4}{\pi\Omega_p^2}\int_0^\infty \omega k(\omega)d\omega, \tag{9}$$

whose ideal values are the atomic number of the element, as well as the perfect-screening (*ps*) sum rule

$$p_{eff} = \frac{2}{\pi}\int_0^\infty \frac{1}{\omega}\mathrm{Im}\left[-1/\varepsilon(\omega)\right]d\omega, \tag{10}$$

whose ideal vale is unity, where $\Omega_p = \sqrt{4\pi n_a e^2/m_e}$ and n_a is the atomic density of the sample, were applied. In Fig. 5, the ELF data are checked by the *f*- and *ps*-sum rules, where we compare Palik's and our present ELF data. Above 120 eV, the ELF data taken from Henke's measurements[48] are used in the evaluation of sum rules. As an intrinsic property, the *f*- and *ps*-sum rules should converge to the theoretical limits being the atomic number and the unit, respectively, when the upper integral limits of Eqs. (8)–(10) become large enough. In the present case, the upper limit is extended to 30 keV, which is higher than the binding energy of the K-shell, with the use of Henke's data. However, it can be seen from Fig. 5(a) that, as the *ps*-sum rule is dominated by the lower energies, the present data occupy almost 98% contribution to the *ps*-sum rule up to 120 eV. While Fig. 5(b) shows that the present data contribute only about 40% to the *f*-sum rule, as in the higher energy loss region, Palik's data are also Henke's data, a comparison of the *f*-sum rule between the present RMC data and Palik's data is still relatively meaningful. The obtained ELF by the RMC method generally is of better accuracy with relative errors being −0.46%, −2.96% and 5.7% for $Z_{eff}|_{ELF}$, $Z_{eff}|_k$ and p_{eff}, respectively, as compared with −7.71%, −10.25% and 5.2% for Palik's data from optical measurements. Though the *ps*-sum rule check is almost the same, the present RMC data perform much better than the Palik's data for the *f*-sum rules. It can be seen from the *f*-sum rule calculations in Figs. 5(b) and 5(c) that the underestimation of about two effective electrons in Palik's data is mainly due to the lower ELF values above the $M_{2,3}$-edge (43–80 eV). Since above this region, the ELF data for Palik's and ours are very close to each other, our data are more accurate and give almost the expected number of effective electrons of Cr. We note that, although theoretically both versions of the *f*-sum rules must converge to the value of the atomic number (24 for Cr) in the high energy loss limit, however, as was stated by Smith and Shiles[49] in their study of *f*-sum rules, generally minor differences should occur compared to the ideal value. In their case of aluminum, data in the x-ray region were neglected in order to reach the expected value of integration. In our case, the small difference may occur from the possible uncertainty of Henke's data in the x-ray energy region.

Applying Eqs. (6) and (7), the optical constants, i.e., the refractive index n and the extinction coefficient k, and the complex dielectric function ε were derived and displayed in Figs. 6 and 7. For comparison, Palik's and Henke's data are

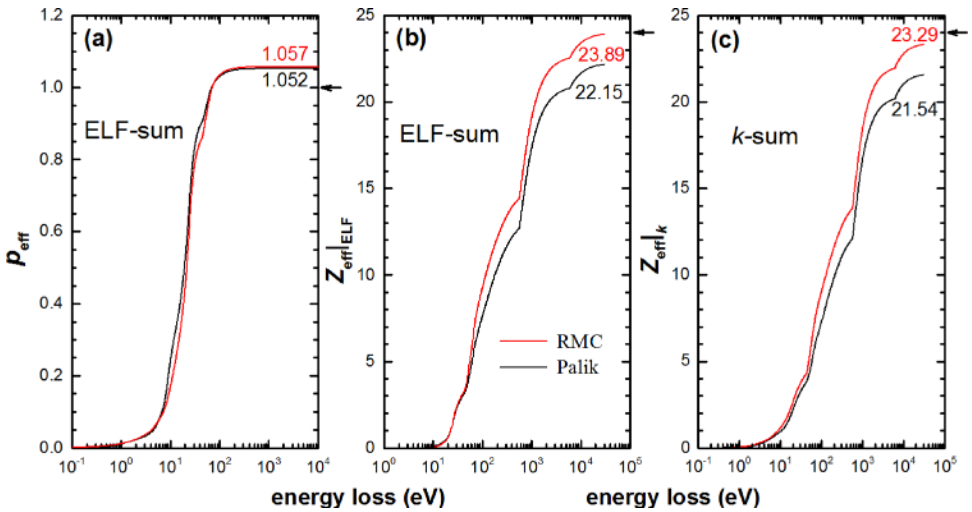

FIG. 5. The *f*- and *ps*-sum rule checks for ELFs of Cr derived from REELS spectra by the RMC method (red line) and from Palik's compiled optical data[2] (black line). (a) The *ps*-sum rule calculated by Eq. (10). (b) The *f*-sum rule calculated by Eq. (8). (c) The *f*-sum rule calculated by Eq. (9). The arrows indicate the ideal values.

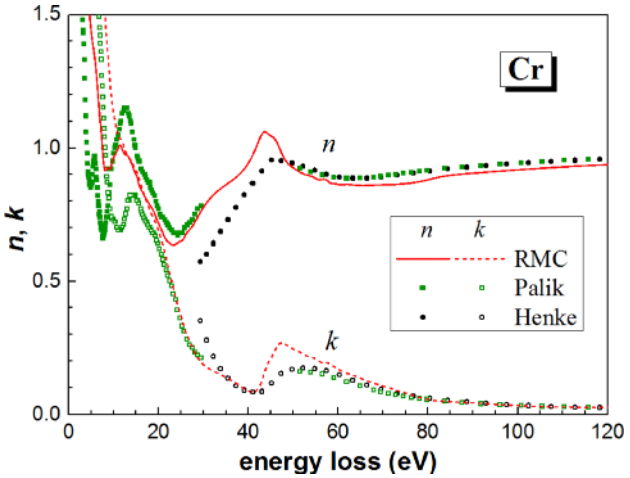

FIG. 6. The refractive index n and the extinction coefficient k of Cr obtained by the RMC method (lines). Palik's[2] (squares) and Henke's data[48] (circles) are shown for comparison.

shown as well. In Fig. 6, a distinct difference in the intensity of the $M_{2,3}$-edge (43–80 eV) of the k-spectra can also be seen among the RMC and the other two measurements. To evaluate the correctness of these data, the f-sum rule regarding k, according to Eq. (9), was calculated and is displayed in Fig. 5(c). For the case of our RMC model, the obtained $Z_{eff}|_k$ is closer to the ideal value. In Fig. 7, the real part of the dielectric function from the optical measurements by Johnson and Christy[50] is also displayed. An extensive peak of the real part of Palik's dielectric function is observed around 1.2 eV (inset of Fig. 7), which was not obtained in the present RMC data. Although it seems that this may be partly due to the broadening of the elastic peak, for the value of the elastic peak in the REELS spectra is ~1.5 eV in Fig. 1, the inset in Fig. 1 indicates that the real elastic peak is limited to ~0.5 eV, and there is no obvious feature around 1 eV. In addition, the current data obtained by the RMC method still show good agreement with the data of Johnson and Christy.

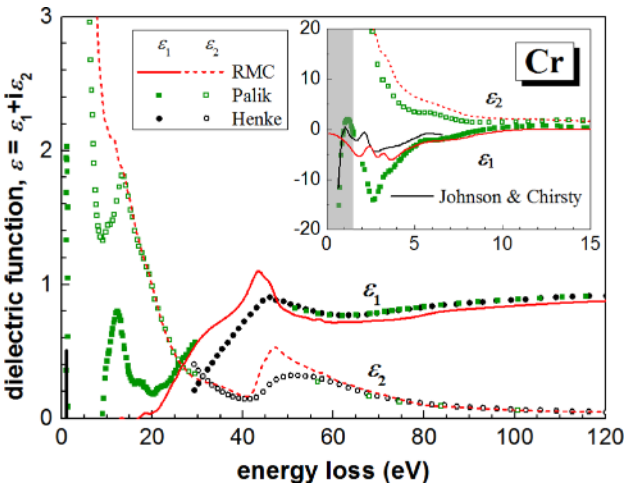

FIG. 7. Comparison of the real and imaginary parts of the complex dielectric function of Cr obtained from the RMC method (lines), and from Palik's[2] (squares) and Henke's data[48] (circles). The inset shows data in the energy loss range of 0–15 eV; the real part of the dielectric function by Johnson and Christy[50] is also displayed. Shadow area in the inset indicates the overly estimated broadening region of the elastic peak in the experimental REELS spectra.

B. Cobalt

In the case of Co, the three ELFs obtained by the RMC method in Fig. 2 were averaged and displayed in Fig. 8. Werner's ELFs[17] determined from the REELS measurements and from first principles calculation based on density functional theory (DFT), as well as those from Palik's[2] and Henke's database,[48] are shown together for comparison. In the whole photon energy range shown, our ELF partially agrees with other datasets. For example, in the low energy loss region (below 18 eV), it agrees with Werner's two ELFs and with Palik's data. In the intermediate region, our ELF agrees either with Werner's ELF from the REELS experiment or with his DFT calculation. Above the $M_{2,3}$-edge threshold (~60 eV), our ELF is nearly the same as Henke's data. On the other hand, Palik's data are generally lower than others, especially in the intermediate energy loss region above 20 eV. Such behavior can be understood from two aspects: (a) the influence of surface contamination and (b) the nearly constant unit value for refractive index n, as is shown in Fig. 10. For a quantitative evaluation of the ELFs, sum rules are evaluated and plotted in Figs. 9(a) and 9(b). Palik's data yield relative errors of −12.4%, −7.1% and −16.9% for $Z_{eff}|_{ELF}$, $Z_{eff}|_k$ and p_{eff}, while they are merely 1.5%, −3.6% and 8.5%, respectively, for the present RMC data. As explained earlier, the ps-sum rule emphasizes more the accuracy of lower energy data, while the f- sum rules emphasize the intermediate and high energy data. However, above 120 eV, there is no difference between the two ELFs; thus, the differences in f- and ps-sum rules between two data are mostly contributed by the difference in ELFs above 20 eV. Therefore, we can conclude that the absolute value of ELF of Co obtained by the RMC analysis of REELS spectra is much more accurate than that by optical methods. For clarification, the sum rules for Werner's data are not shown here,

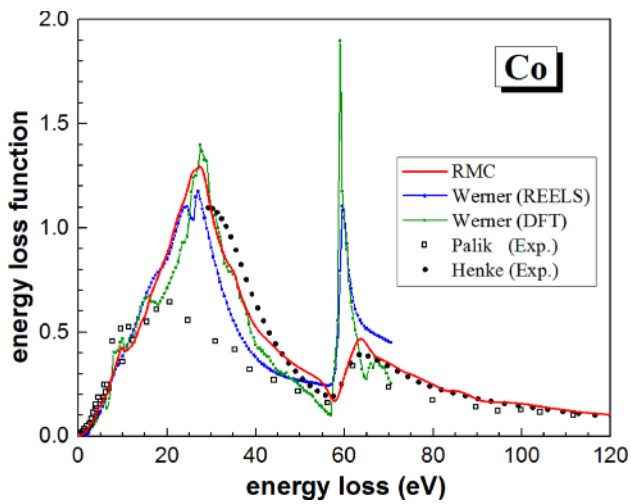

FIG. 8. Comparison of the ELFs of Co. Red line: present results obtained from the REELS measurement by the RMC method; blue dotted line: ELF from Werner's REELS data; green dotted line: ELF from Werner's DFT calculation;[17] open square: optical measurements compiled in Palik's database;[2] and solid circle: from Henke's atomic scattering factors.[48]

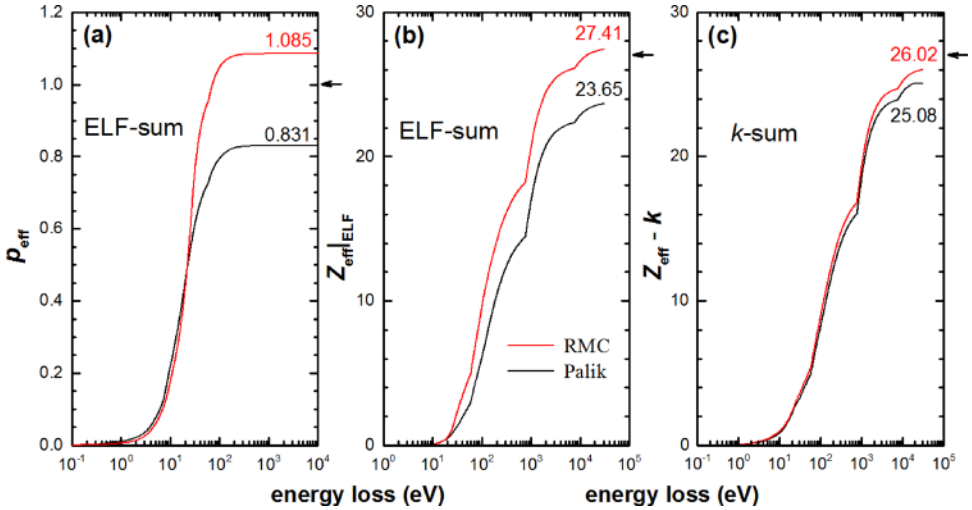

FIG. 9. The *f*- and *ps*-sum rule checks for ELFs of Co derived from REELS spectra by the RMC method (red line) and from Palik's compiled optical data[2] (black line). (a) The *ps*-sum rule calculated by Eq. (10). (b) The *f*-sum rule calculated by Eq. (8). (c) The *f*-sum rule calculated by Eq. (9). The arrows indicate the ideal values.

simply because their ELFs were scaled so as to satisfy both the *f*- and *ps*-sum rules.[17] A common feature of Werner's ELFs is that both the REELS and DFT data have very strong intensities at the $M_{2,3}$-edge, which has not been found in other data sources. It is clearly seen that this edge peak in the REELS spectrum is not so sharp, either from Fig. 2(a) or from Fig. 13 in Ref. 17.

From Eqs. (6) and (7), the optical constants and the complex dielectric function ε are derived and displayed in Figs. 10 and 11, respectively. For comparison, Palik's and Henke's data are shown as well. One good evidence to show the validity of the RMC model is that, although significant discrepancies between the ELFs of Palik's and ours exist (see Fig. 8), the relevant extinction coefficients *k* (see Fig. 10) are almost the same above 40 eV. Moreover, at the high energy limit, the $Z_{eff}|_k$ value calculated with the present results of *k* is closer to the ideal value than with Palik's data. Therefore, the discrepancy between our present ELF and Palik's ELF mostly resulted from the refractive index in a large photon energy range of Palik's data. We also note that we found very good agreement between Palik's data and the RMC data in the low energy loss region, as is shown in the inset of Fig. 11, for the complex dielectric function. This indicates that in the region below 10 eV, both the *n* and *k* values by Yu *et al.*[51] are sufficiently accurate.[2]

C. Palladium

In the case of Pd, the ELFs derived by different groups are more scattered than in cases of Cr and Co. As was stated in Palik's Handbook,[2] the optical constants of Pd depend on the sample preparation, accuracy of the optical measurement and the method by which the experimental data are analyzed. To sum up, only the general tendency of ELFs exists among different data sources, as shown in Fig. 12, where the present RMC-ELF was obtained by taking average over primary energies of 2000, 3000 and 4000 eV in Fig. 3. In Fig. 12, a

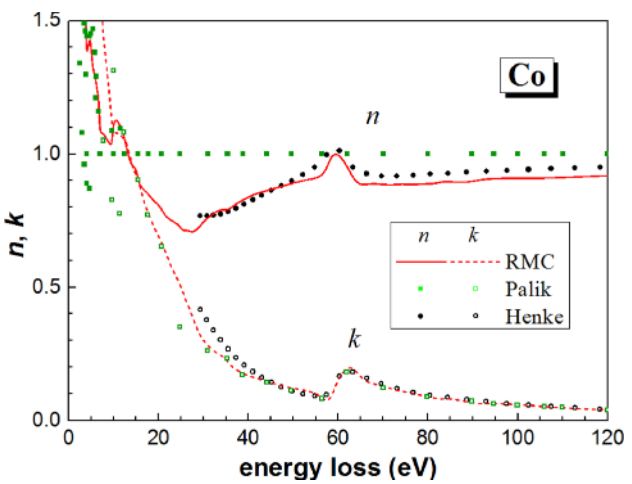

FIG. 10. The refractive index *n* and the extinction coefficient *k* of Co obtained by the RMC method (lines). Palik's[2] (squares) and Henke's data[2] (circles) are shown for comparison. Palik's data are compiled from several different sources.

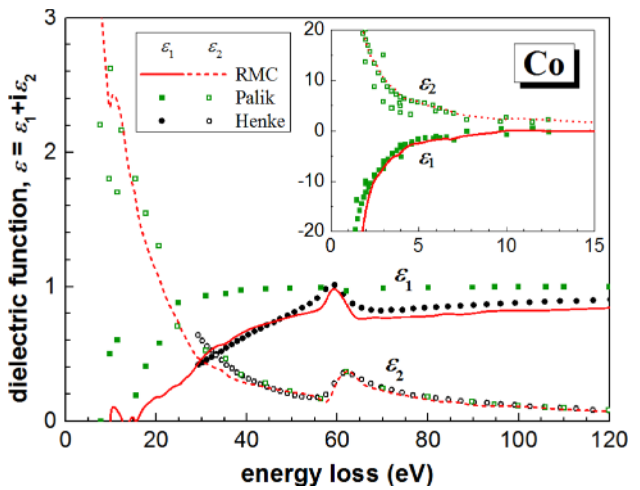

FIG. 11. Comparison of the real and imaginary parts of the complex dielectric function of Co obtained from the RMC method (lines), and from Palik's[2] (squares) and Henke's database[48] (circles). The inset shows data in the energy loss range of 0–15 eV.

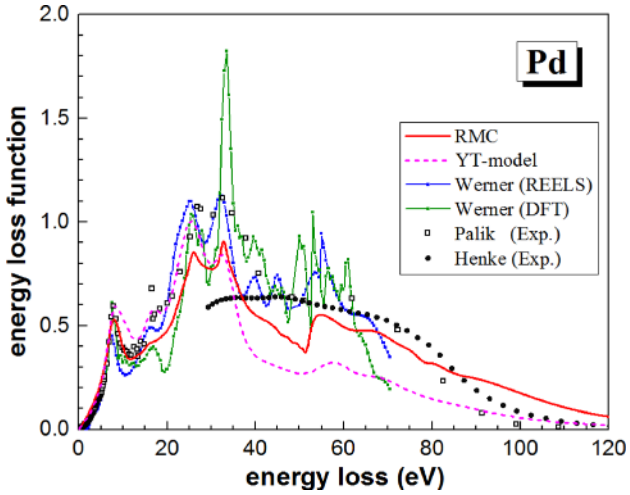

FIG. 12. Comparison of ELFs of Pd obtained from REELS measurements by the RMC method in this work (red line), with the ELF obtained from the YT model (dash line),[15] Werner's REELS data and DFT calculation (dotted line),[17] optical measurements compiled in Palik's database[2] (open square) and from Henke's atomic scattering factors[48] (solid circles).

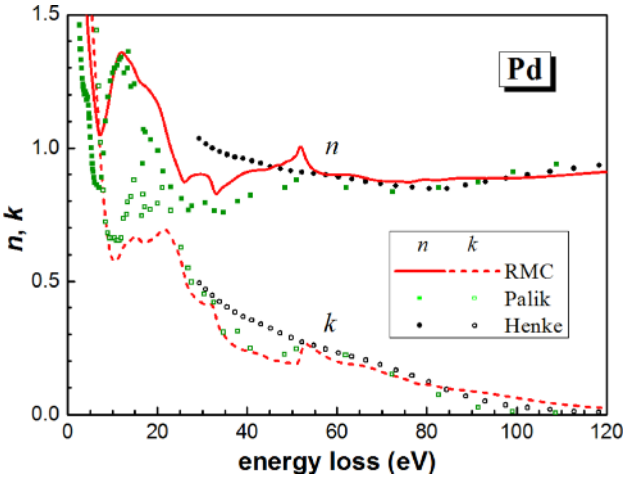

FIG. 14. The refractive index n and the extinction coefficient k of Pd obtained by the RMC method (lines). Palik's[2] data (squares) and Henke's data[2] (circles) are shown for comparison.

unique feature of Werner's DFT-ELF demonstrates fluctuations, especially in the intermediate energy loss region near the $N_{2,3}$-edge. Other data sources have relatively smooth ELFs. By the YT model and the RMC method, the $N_{2,3}$-edge threshold around 51 eV is more clear than other ELFs. Using the ELF obtained by our RMC model, the threshold energy of the $N_{2,3}$-edge is evaluated as 50.9 eV, which is identical to the energy determined by photoelectron spectroscopy.[52] In Figs. 13(a) and 13(b), the *f*- and *ps*-sum rules are displayed to test the ELFs calculated from our RMC model with a linear interpolation with Henke's data after 120 eV, from Palik's data and from the YT model. The Palik's ELF has relative errors of −2.5%, and 13.1% for *f*- and *ps*-sum rules, respectively. This indicates that Palik's ELF is overestimated in the low energy loss region and is underestimated in the intermediate and high energy loss regions. Since the ELF by the YT model was normalized with the *ps*-sum rule,[15] the *ps*-sum rule almost gives the ideal value of 1. However, as mentioned in the Introduction, the ELF by the YT model does not always behave well in the *f*-sum rule check. In the case of Pd, the *f*-sum rule integration result is 39.42, and therefore at least 6 effective electrons were not correctly accounted for in the ELF. In contrast, the RMC-ELF behaves very well for both sum rules, with relative errors of −1.6%, and 4.3% for *f*- and *ps*-sum rules, respectively. For comparison, the optical constants and the complex dielectric function of Pd derived from the RMC data are shown in Figs. 14 and 15, respectively, with Palik's and Henke's data. To sum up, the RMC data are in moderate agreement with Palik's data in the low energy loss region, while in the high energy loss region, they agree with both Palik's and Henke's data. It is worth mentioning that for the extinction function k and the imaginary part of the dielectric function, the RMC data agree well with Palik's data in almost the whole energy loss region studied. This partly indicates that data for the refractive index n of Palik's are not as accurate as the extinction

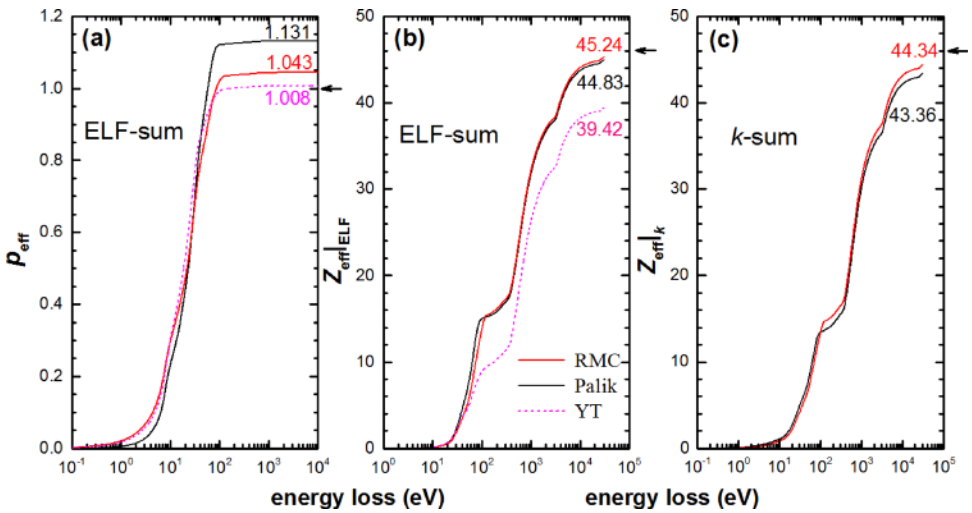

FIG. 13. The *f*- and *ps*-sum rule checks for ELFs of Pd derived from REELS spectra by the RMC method (red line), from Palik's compiled optical data[2] (black line) and from the YT model (magenta line).[15] (a) The *ps*-sum rule calculated by Eq. (10); (b) the *f*-sum rule calculated by Eq. (8); and (c) the *f*-sum rule calculated by Eq. (9). The arrows indicate the ideal values.

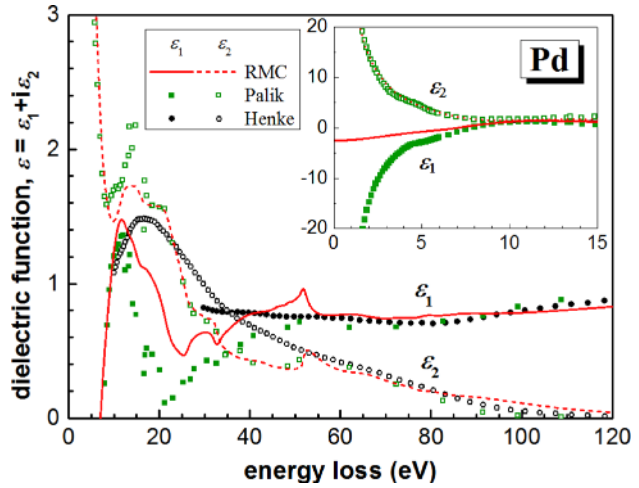

FIG. 15. Comparison of the real and imaginary parts of the complex dielectric function of Pd obtained from the RMC method (lines) and from Palik's[2] (squares) and Henke's database[48] (circles). The inset shows data in the energy loss range of 0–15 eV.

coefficient k. In Fig. 13(c), the f-sum rule for the extinction coefficient was calculated, where the relative errors for the theoretical limit (atomic number of Pd, 46) were determined to be −5.7% for the Palik data and −3.6% for the RMC results. Therefore, in the inset of Fig. 15, the deviation in the real parts of the dielectric function of the RMC data and the Palik data can be understood as a result of the discrepancies in the refractive index n. We can conclude that the current ELF and optical constants determined by the RMC method are obtained with higher accuracy, as indicated by the sum rules.

V. CONCLUSION

In summary, we have calculated the ELFs and the optical constants of three transition metals, Cr, Co, and Pd, in the photon energy range of 0–120 eV from the analysis of three REELS spectra at three primary energies. A recently developed RMC method was applied to extract the absolute ELF values from each REELS spectrum, where a Monte Carlo simulation of electron scattering in the REELS experiment and a global optimization technique for oscillator parameter fitting were employed. With implementation of a spatially varying DIIMFP derived under the semi-classical framework for electron inelastic scattering and Mott's cross-section for electron elastic scattering, an accurate description of electron transport was established for the REELS spectral analysis. The validity of the obtained ELF of the RMC method has been confirmed by the fairly good performance of the f- and ps-sum rule checks and by good consistency of the ELFs obtained at different primary energies. This work then proves that the RMC method with REELS spectra enables establishing a database of optical constants for many materials at a higher accurate level than the previous databases.

ACKNOWLEDGMENTS

This work was supported by the National Natural Science Foundation of China (Grant No. 11574289) and Special Program for Applied Research on Super Computation of the NSFC-Guangdong Joint Fund (2nd phase) under Grant No. U1501501, the National Research, Development and Innovation Office (NKFIH) under Grant KH 126886 and the European Cost Actions CA15107 (MultiComp) and MP1306 (MPNS). We are thankful to Dr. Andrew Cheesman for the critical reading of the manuscript. We also thank Dr. H. M. Li and the supercomputing center of USTC for their support in performing parallel computations.

[1]E. D. Palik, *Handbook of Optical Constants of Solids* (Academic Press, New York, 1985).
[2]E. D. Palik, *Handbook of Optical Constants of Solids* (Academic Press, New York, 1991), Vol. 2.
[3]J. Daniels, C. V. Festenberg, H. Raether, and K. Zeppenfeld, *Optical Constants of Solids by Electron Spectroscopy* (Springer, New York, 1970), pp. 77–135.
[4]R. F. Egerton, *Electron Energy Loss Spectroscopy in the Electron Microscope*, 2nd ed. (Plenum Press, New York, 1986).
[5]C. Werenkel and B. Gauthé, Phys. Status Solidi B **64**, 515 (1974).
[6]Y. Ohno, Phys. Rev. B **39**, 8209 (1989).
[7]J. C. Ingram, K. W. Nebesny, and J. E. Pemberton, Appl. Surf. Sci. **44**, 279 (1990).
[8]F. Yubero, J. M. Sanz, E. Elizalde, and L. Galan, Surf. Sci. **237**, 173 (1990).
[9]F. Yubero, S. Tougaard, E. Elizalde, and J. M. Sanz, Surf. Interface Anal. **20**, 719 (1993).
[10]H. Yoshikawa, Y. Irokawa, and R. Shimizu, J. Vac. Sci. Technol. A **13**, 1984 (1995).
[11]T. Nagatomi, T. Kawano, and R. Shimizu, J. Appl. Phys. **83**, 8016 (1998).
[12]W. S. M. Werner, Appl. Phys. Lett. **89**, 213106 (2006).
[13]H. Jin, H. Shinotsuka, H. Yoshikawa, H. Iwai, S. Tanuma, and S. Tougaard, J. Appl. Phys. **107**, 083709 (2010).
[14]B. Da, Y. Sun, S. F. Mao, Z. M. Zhang, H. Jin, H. Yoshikawa, S. Tanuma, and Z. J. Ding, J. Appl. Phys. **113**, 214303 (2013).
[15]D. Tahir, J. Kraaer, and S. Tougaard, J. Appl. Phys. **115**, 243508 (2014).
[16]S. Tougaard and I. Chorkendorff, Phys. Rev. B **35**, 6570 (1987).
[17]W. S. M. Werner, K. Glantschnig, and C. Ambrosch-Draxl, J. Phys. Chem. Ref. Data **38**, 1013 (2009).
[18]W. S. M. Werner, Surf. Sci. **526**, L159 (2003).
[19]F. Yubero and S. Tougaard, Phys. Rev. B **46**, 2486 (1992).
[20]F. Yubero, J. M. Sanz, B. Ramskov, and S. Tougaard, Phys. Rev. B **53**, 9719 (1996).
[21]F. Yubero, N. Pauly, A. Dubus, and S. Tougaard, Phys. Rev. B **77**, 245405 (2008).
[22]S. Hajati, O. Romanyuk, J. Zemek, and S. Tougaard, Phys. Rev. B **77**, 155403 (2008).
[23]D. Tahir and S. Tougaard, J. Phys.: Condens. Matter **24**, 175002 (2012).
[24]N. Pauly, F. Yubero, J. P. Espinos, and S. Tougaard, Appl. Opt. **56**, 6611 (2017).
[25]N. F. Mott, Proc. R. Soc. London A **124**, 425 (1929).
[26]N. F. Mott, Nature **124**, 986 (1929).
[27]F. Yubero and S. Tougaard, Surf. Interface Anal. **19**, 269 (1992).
[28]H. Xu, B. Da, J. Tóth, K. Tőkési, and Z. J. Ding, Phys. Rev. B **95**, 195417 (2017).
[29]H. Xu, L. H. Yang, B. Da, J. Tóth, K. Tőkési, and Z. J. Ding, Nucl. Instrum. Methods B **406**, 475 (2017).
[30]B. Da, S. F. Mao, and Z. J. Ding, J. Phys.: Condens. Matter **23**, 395003 (2011).
[31]Y. C. Li, Y. H. Tu, C. M. Kwei, and C. J. Tung, Surf. Sci. **589**, 67 (2005).
[32]L. Kövér, D. Varga, I. Cserny, J. Tóth, and K. Tökési, Surf. Interface Anal. **19**, 9 (1992).
[33]J. Chastain, R. C. King, and J. Moulder, *Handbook of X-ray Photoelectron Spectroscopy: A Reference Book of Standard Spectra for Identification and Interpretation of XPS Data* (Physical Electronics Division, Perkin-Elmer Corporation Eden Prairie, Minnesota, 1992).
[34]J. Toth, J. Surf. Anal. **1**, 101 (1995).
[35]Y. Yamazaki, "Studies on electron scattering by mercury atoms and electron spin polarization detector," Ph.D. thesis (Osaka University, 1977).
[36]R. A. Bonham and T. G. Strand, J. Chem. Phys. **39**, 2200 (1963).

[37]C. J. Tung, Y. F. Chen, C. M. Kwei, and T. L. Chou, Phys. Rev. B **49**, 16684 (1994).
[38]Y. F. Chen and C. M. Kwei, Surf. Sci. **364**, 131 (1996).
[39]A. C. Simonsen, F. Yubero, and S. Tougaard, Phys. Rev. B **56**, 1612 (1997).
[40]Y. F. Chen, Phys. Rev. B **58**, 8087 (1998).
[41]Z. J. Ding, J. Phys.: Condens. Matter **10**, 1733 (1998).
[42]Z. J. Ding, J. Phys.: Condens. Matter **10**, 1753 (1998).
[43]Z. J. Ding and R. Shimizu, Phys. Rev. B **61**, 14128 (2000).
[44]A. Rivacoba and P. M. Echenique, Scanning Microsc. **4**, 1 (1990).
[45]A. Rivacoba, N. Zabala, and J. Aizpurua, Prog. Surf. Sci. **65**, 1 (2000).
[46]R. H. Ritchie and A. Howie, Philos. Mag. **36**, 463 (1977).
[47]S. Kirkpatrick, C. D. Gelatt, and M. P. Vecchi, Science **220**, 671 (1983).
[48]B. L. Henke, E. M. Gullikson, and J. C. Davis, At. Data Nucl. Data Tables **54**, 181 (1993).
[49]D. Y. Smith and E. Shiles, Phys. Rev. B. **17**, 4689 (1978).
[50]P. Johnson and R. Christy, Phys. Rev. B **9**, 5056 (1974).
[51]A. C. Yu, T. M. Donovan, and W. E. Spicer, Phys. Rev. **167**, 670 (1968).
[52]J. C. Fuggle and N. Mårtensson, J. Electron Spectrosc. **21**, 275 (1980).